

## Solar Total Eclipse of 21 August 2017: Study of the Inner Corona Dynamical Events Leading to a CME

Boris Filippov<sup>1,2</sup> · Serge Koutchmy<sup>2</sup> ·  
Nicolas Lefaudeux<sup>2,3</sup>

© Springer ●●●

**Abstract** Total solar eclipse (TSE) coronal large and small scale events were reported in the historical literature but a definite synoptic coverage was missing for studying a relationship with the more general magnetic context of the solar-disk. We here analyze temporal changes in the solar corona before, during, and after the total solar eclipse on 21 August 2017 from a set of ground-based and of space-borne observations. High-quality ground-based white-light (W-L) observations and a deep image processing allow us to reveal these changes for the first time with a fraction of a one-minute time resolution. Displacements of a number of fine coronal features were measured for the first time at these small radial distances, using a diffraction limited instrument at a single site. The comparison with space-based observations, including observations from the *Solar Terrestrial Relations Observatory* (STEREO) mission, showed that the features belong to a slow coronal mass ejection (CME) propagating through the corona with the nearly constant speed of  $250 \text{ km s}^{-1}$ . Our TSE images provide the same typical velocity as measured at a distance of one solar radius from the surface. The event was initiated by coronal dynamics manifested by a prominence eruption that started just before the eclipse observations and an ascent of a U-shaped structure visible in the AIA 171 Å channel, which we assume as the lower part of a coronal cavity. The prominence material was observed draining down towards

---

✉ B. Filippov  
bfilip@izmiran.ru  
S. Koutchmy  
koutchmy@iap.fr  
N. Lefaudeux  
nicolas.lefaudeux@gmail.com

- <sup>1</sup> Pushkov Institute of Terrestrial Magnetism, Ionosphere and Radio Wave Propagation, Russian Academy of Sciences, Troitsk, Moscow, 108840, Russia
- <sup>2</sup> Institut d'Astrophysique de Paris, CNRS and Sorbonne University, UMR 7095, 98 Bis Boulevard Arago, 75014 Paris, France
- <sup>3</sup> Imagine Eyes, 18 rue Charles de Gaulle, 91400 Orsay, France

the chromosphere along the prominence arch. While the prominence disappears in the STEREO-A field-of-view at the height of about  $6'$  above the limb, the corresponding flux rope seems to continue towards the outer corona and produces the slow CME with turbulent motion. The overall mass of the moving features is evaluated based on absolute photometrical data extracted from our best W-L eclipse image.

**Keywords:** Corona, Structures; Coronal Mass Ejections, Low Coronal Signatures; Eclipse Observations; Prominences, Active;

## 1. Introduction

Coronal mass ejections (CMEs) were observed for the first time in the early 1970s from space-borne observations of the *Orbiting Solar Observatory* (OSO)-7 coronagraph (Tousey, 1973) and were called “coronal transients”. The following generations of space-borne coronagraphs drastically enlarged the knowledge of the phenomenon. It was proved that these observed transient changes in the structure of the solar corona really represent mass motions in space (Wagner, 1984; Schwenn, 1996) supported by changes near the solar surface.

In past eclipse observations, there was a chance to discover a large scale dynamical coronal event. If a CME were well outlined in the coronal structure and observations were made at different places far along the Moon-shadow path, the comparison of two eclipse images could provide information about moving features. However, CMEs were not really discovered before the space era (Wagner, 1984). There are structures in drawings of the corona made in the 19th century that nowadays could be considered as CMEs (Bugoslavskaja, 1949; Eddy, 1974; Cliver, 1989), but they did not attract too much attention and were not recognized as moving. The best eclipse coronal event we found, on 21 September 1941, was analyzed in the little-known Bugoslavskaja (1949) work dealing with coronal structures. The introduction of the work gives an excellent account of historical eclipse observations suggesting dynamical phenomena at a time when the true high-temperature nature of the corona was not yet fully recognized. For this well-observed 1941 eclipse event, her Figure 49 shows the proper motion map of the prominence during the event; the motion of fine white-light (W-L) coronal details (loops, front, rays) in the inner corona is also of great interest, see Figure 1a. Her Table 15 giving a large number of observed parameters, including the measured displacements from several plates separated in time by an interval up to nine minutes, convincingly demonstrates that a coronal event with complex interlaced loops and rays showing outwards velocities of  $10$  to  $50 \text{ km s}^{-1}$ , are connected to the dynamical behaviour of the underlying prominence; see Figure 1a. Rapid variations in the coronal structure were indeed recorded as early as the 1973 total solar eclipse (TSE) in images obtained with a two-hour interval (Koutchmy and Fagot, 1973).

Another historical observation of a large eclipse CME event called a transient event was reported from the analysis of pictures obtained 27 minutes apart and 90 minutes apart during the 15 February 1980 TSE, see Figure 1b taken from

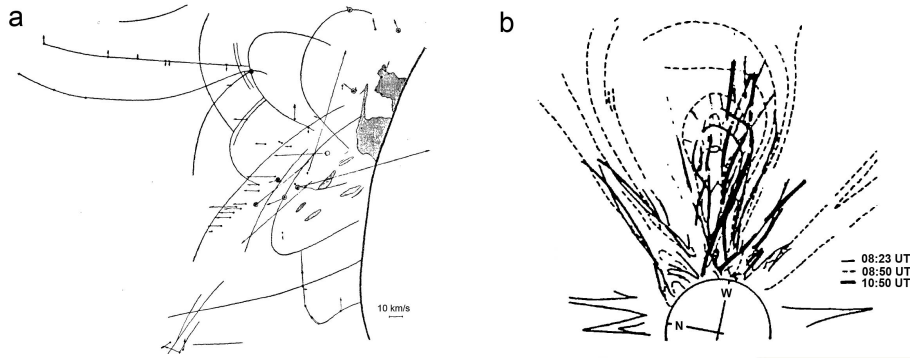


**Figure 1.** *Left:* Historical observation of the TSE coronal event of 21 September 1941 with slow expansion of coronal loops and rays above an activated prominence. The bar at the bottom right corresponds to a proper motion of  $10 \text{ km s}^{-1}$ . The prominence dynamics were discussed separately but one can note the prominence remnants of cool material just under a W-L front with expansion suggesting a synchronized eruption. Eclipse multi-station observations and analysis by Bugoslavskaja (1949). *Right:* The so-called “tennis racket” CME event observed during the 15 February 1980 TSE; drawing made from large scale pictures (Airapetian and Koutchmy (1994), Figure 2B, with permission of the authors).

the Airapetian and Koutchmy (1994) report. This event was called, in the citizen science literature relating TSE observations, the “tennis racket event”. Twisted diverging legs were suggested by Airapetian and Koutchmy (1994) from the visual interpretation of the processed pictures, with a possible reconnection occurring in the low part of the twisted loop as the result of a kink instability; large velocities were measured higher up, typically  $400$  to  $800 \text{ km s}^{-1}$  depending of the radial distance. Only low-resolution-photographic pictures without space-based observations were available on 15 February 1980. However this photographic observation suggested quite convincingly that the apparent bubble-like configuration of a CME does not hold in 3D because a twisted flux rope was identified at large scale.

More recently, an eclipse CME was well described by Koutchmy *et al.* (2004). It occurred during the 11 August 1999 widely observed eclipse corona near the maximum of activity. At the W-limb a large prominence cavity system evolves; rather large velocities ( $440 \text{ km s}^{-1}$ ) were reported from the Large Angle and Spectrometer Coronagraph (LASCO: Brueckner *et al.*, 1995) C2 W-L observations onboard the *Solar and Heliospheric Observatory* (SOHO). The authors developed a great deal of attention to the phenomenon of expansion observed in the high arch overlying the erupting part of the prominence without reaching a definite conclusion about the origin of the large CME, although some evidence of a reconnecting phenomenon was given based on a sequence of the processed filtergrams taken by the Extreme-ultraviolet Imaging Telescope (EIT: Delaboudinière *et al.*, 1995) onboard SOHO.

At the time of the following solar maximum, Hanaoka *et al.* (2014) analyzed again some eclipse CMEs seen at both limbs of the eclipse corona of 13 November 2012, using two sets of images taken 35 minutes apart. At the E-limb a rather faint bubble-like CME related to a flare was studied showing a velocity of the

front of  $360 \text{ km s}^{-1}$  in the region one solar radius ( $R_{\odot}$ ) from the limb, which is low for a solar maximum CME. At this well-observed eclipse, many observations were taken from Australia, but unfortunately the CMEs were not noticed although they were well recorded afterwards with the LASCO coronagraphs. At the W-limb the unique eclipse pictures of Hanaoka *et al.* (2014) show the motion of a system of arches that the authors identified with a conventional CME case appearing after a prominence eruption with a dark cavity moving outwardly. The proper motions were typically  $10 \text{ km s}^{-1}$  in the inner corona region and  $130 \text{ km s}^{-1}$  in the  $1 R_{\odot}$  region. They called the event a “hot-air balloon loop structure” and proposed to identify it with the initiation region of the CME as shown by the eclipse pictures. The corresponding SOHO/LASCO CME was seen with velocities of  $130 \text{ km s}^{-1}$  at the height of  $4-5 R_{\odot}$  which makes it definitely a slow CME observed at solar maximum. Similar “balloon-like” structures were observed previously (*e.g.* Srivastava *et al.*, 1999, 2000).

During the TSE of 2013, two large prominent CMEs extending far into the corona can be seen in the coronal image of 03 November 2013 ([www.zam.fme.vutbr.cz/~druck/Eclipse/Ecl2013g/TSE\\_2013c2\\_ed/Hr/TSE\\_2013c2\\_ed.png](http://www.zam.fme.vutbr.cz/~druck/Eclipse/Ecl2013g/TSE_2013c2_ed/Hr/TSE_2013c2_ed.png)). The eclipse reconstructed image is a result of a sophisticated digital processing of many coronal images taken with different exposures at the observation site using the M. Druckmüller’s method (Druckmüller, Rušin, and Minarovjeh, 2006). The CMEs can be easily recognized in the processed image and compared with space-based coronagraphic observations. However, the authors did not use a method that would allow detecting a CME motion or even small changes in the structure of the corona during the short time of totality at a particular observation site from the same instrument. No space-based observations of the same CME were analyzed as far as we know.

The CME speed in the sky plane varies in a wide range from tens to more than  $2500 \text{ km s}^{-1}$ , with an average value of about  $500 \text{ km s}^{-1}$  (Gopalswamy, 2004). CMEs with lower than the average speed can be considered as slow (Boulade *et al.*, 1997), while the others are fast. Sheeley *et al.* (1999) suggested that slow, or as they call them gradual CMEs, accelerate within the coronagraph field-of-view (FOV) and in most cases are associated with filament eruptions. Slow CMEs with persistently weak acceleration are known also as balloon-type events (Srivastava *et al.*, 1999, 2000). Fast, or impulsive, CMEs, in contrast, usually decelerate and are related to solar flares. However, the separation of CMEs into two groups is rather arbitrary because parameters of flare-associated and non-flare CMEs considerably overlap (Vršnak, Sudar, and Ruždjak, 2005) and in most energetic events both flares and filament eruptions are observed (*e.g.* Schmieder, Aulanier, and Vršnak, 2015). Many researchers agree that one mechanism is sufficient to explain flare-related and prominence-related CMEs (Chen and Krall, 2003; Feynman and Ruzmaikin, 2004).

The typical morphological structure of a CME consists of three parts: a bright frontal loop followed by a dark cavity with an embedded bright core representing remnants of an eruptive filament (House *et al.*, 1981; Illing and Hundhausen, 1985). The CME dark cavities result from the development of coronal cavities observed in W-L, extreme ultraviolet (EUV), and soft X-ray emission around prominences and at the feet (bases) of coronal streamers (Gibson *et al.*, 2006;

Habbal *et al.*, 2010; Kucera *et al.*, 2012; Reeves *et al.*, 2012; Karna, Pesnell, and Zhang, 2015). It is widely assumed that the cavity represents a magnetic flux rope with helical magnetic field. The lowest sections of the helices, dips, can be filled with colder dense plasma of a prominence. Prominence material is sometimes observed as highly twisted structures in the core of CMEs (Boulade *et al.*, 1997; Li and Zhang, 2015).

A CME cannot be characterized by a unique speed. Different parts of the CME move with different speeds. The fastest part of the CME is the frontal loop; the core moves slower (Zhang *et al.*, 2001; Foley *et al.*, 2003; Cheng *et al.*, 2014). The bottom edge of the cavity moves with the lowest speed (Vršnak *et al.*, 2004). This is the consequence of the composition of the flux rope in two motions: a translational ascending motion and a radial expansion. Finally, in the framework of the study of slow and “weak” CMEs, let us note the analysis of events that are a component of the coronal dynamics possibly related to the so-called slow wind. Such components are now called “blobs” (Sheeley and Wang, 2007).

In this article, we present the results of a specially designed imaging W-L experiment performed during the TSE observations on 21 August 2017. Definite traces of the propagation of a slow CME inside the W-L corona are reported during the totality. Multi-wavelength observations with space-based instruments are also used to study the evolution of the coronal region under interest before, during, and after the totality. The CME was initiated by a very slow filament eruption and moved later with a constant speed.

## 2. Observations

W-L eclipse observations we used were made on the west coast of the United States near Unity, Oregon near 17:24 UT. A special algorithm to make high quality High Dynamic Range (HDR) composite images was used. The High dynamic range (HDR) imaging methods have been developed for a long time (see, *e.g.*, Banterle *et al.*, 2018). For processing eclipse coronal images the most popular algorithm was developed by Milo Druckmüller in Brno (Druckmüller, Rušin, and Minarovjech, 2006) (see also his website [www.zam.fme.vutbr.cz/~druck/Eclipse/](http://www.zam.fme.vutbr.cz/~druck/Eclipse/)). Excellent reproductions of images are provided in the website at [hdr-astrophotography.com/](http://hdr-astrophotography.com/) as well as a view of the equipment used. Some selected original images are available from the site: [bass2000.obspm.fr/piwigo/index.php?category/141](http://bass2000.obspm.fr/piwigo/index.php?category/141). In addition, EUV coronal images taken by the Atmospheric Imaging Assembly (AIA: Lemen *et al.*, 2012) onboard the *Solar Dynamic Observatory* (SDO) and the Sun Earth Connection Coronal and Heliospheric Investigation (SECCHI) Extreme Ultraviolet Imager (EUVI: Wuelser *et al.*, 2004; Howard *et al.*, 2008) onboard the *Solar Terrestrial Relations Observatory* (STEREO) are used. W-L images obtained with the SOHO/LASCO were analysed for the CME evolution in the more outer corona.

The high-quality W-L coronal images allowed us to recognize a number of small coronal features moving outward in the south-east sector of the corona (Movie1) during the short period of the totality ( $\approx 1$  minute 45 seconds). Frames in Movie1 run forth and back for better visibility of the moving features. They

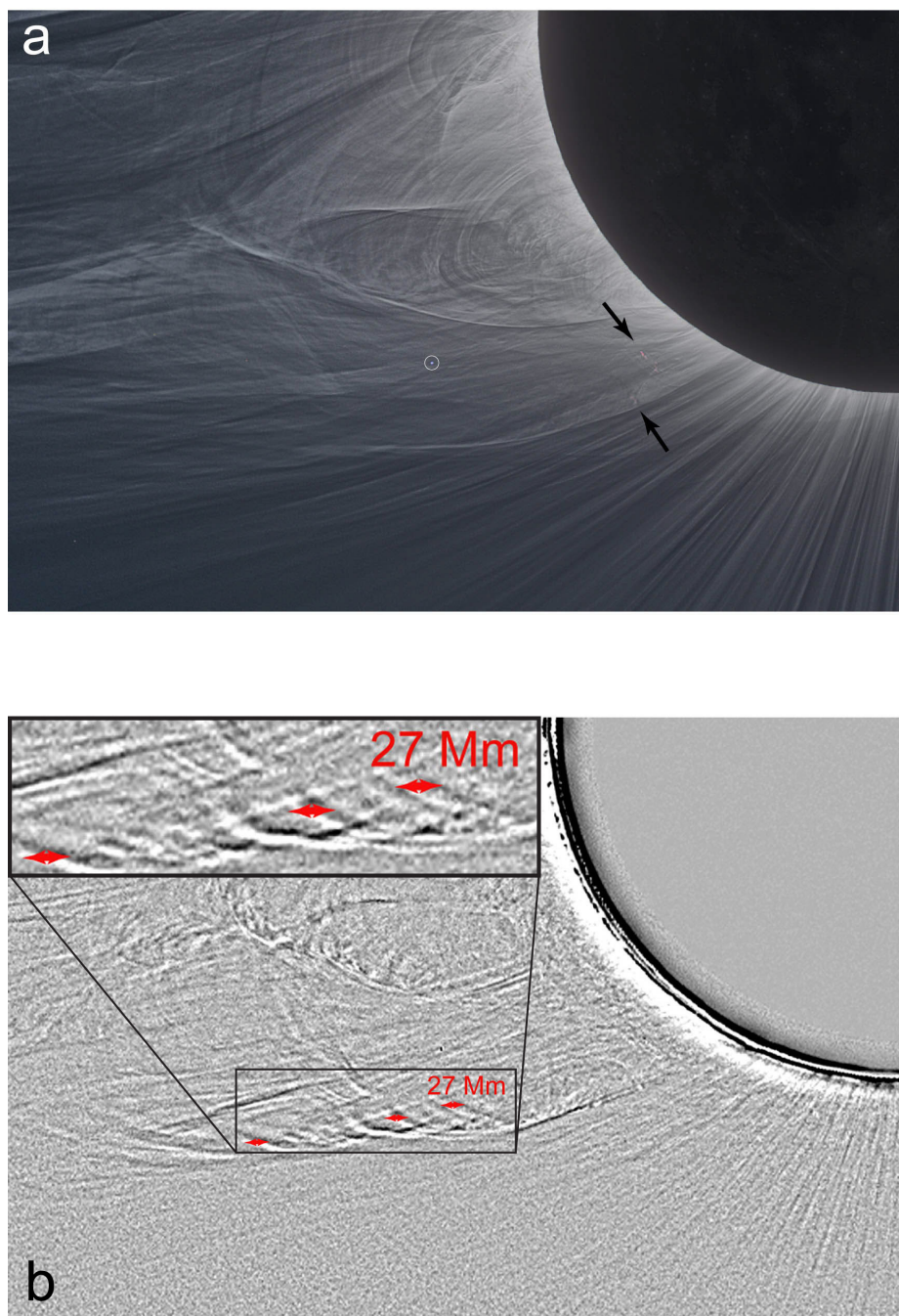


**Figure 2.** Partial frame of the ground-based coronal image on 21 August 2017 at 17:24 UT made using a deep-processing technique to show fine coronal structures (**a**), difference image of the corona with a time lapse of 1.75 minutes (**b**). *Black arrows* in (**a**) point to the eruptive prominence remnants observed as reddish features owing to  $H\alpha$  and  $D_3$  emissions. *Red arrows* in (**b**) indicate the displacement of coronal structures during the totality. The small white dot surrounded by the *thin white circle* near the centre of the upper frame is the image of a star not seen after making the subtraction as seen in the lower frame, in contrast to the lunar limb showing a large displacement (see also the Electronic Supplementary Material, Movie 1).

are hardly noticeable in a particular static coronal image (Figure 2a) and it is unlikely that their changes could be identified in images taken at different places along the Moon-shadow path. Only an examination of a movie or a difference of images taken at the beginning and at the end of the totality (Figure 2b) using the same instrumental set-up and the same image processing allow us to find the changes in the fine coronal structure. The displacement of the best identified features in the vicinity of radial distances  $\approx 1.8 R_{\odot}$  is about 27 Mm as is shown in Figure 2b by red arrows. The speed of the feature motion is about  $250 \text{ km s}^{-1}$ . In order to find the cause and source of this motion, we analyzed observations of the Sun in different wavelengths made by different space missions.

### 3. Prominence Dynamics

Several hours before the totality observed at 17:24 UT, a prominence activation started in the south-east sector of the solar limb. It was observed in the  $304 \text{ \AA}$  channel of SDO/AIA (Figures 3 and 4, Movie 2) but was more impressively visible in the  $304 \text{ \AA}$  channel of STEREO/EUVI (Figures 5 and 6, Movie 3). STEREO Ahead (STA) was at the  $128^{\circ}$  separation angle with Earth, and the prominence was in the south-west sector of the limb in its images. The prominence belonged to a family of polar crown prominences elongated along the heliographic parallel (East-West direction) at a latitude of about  $S40^{\circ}$ . The top of the prominence shifted most noticeably both in the SDO FOV and STA FOV in the direction parallel to the Equator. That is why we will analyse the motion in this direction and will refer below to the distance from the prominence top to the limb along this direction as the projected height, if it is not stated otherwise. At the beginning of the activation at 13:00 UT the projected prominence height above the limb was about 100 Mm in the AIA FOV and about 25 Mm in the EUVI FOV. If we observe the same point of the prominence spine with each instrument, we can estimate its latitude using the expression for the projected height of a feature above the limb at the latitude  $\phi$  (*e.g.* Filippov, 2013)

$$h = (H + R_{\odot} \cos \phi) \sin \lambda - R_{\odot} \cos \phi, \quad (1)$$

where  $h$  is the projected height of the feature above the limb,  $H$  is the true distance from the feature to the surface along the line parallel to the equator, and  $\lambda$  is its longitude, the angle between the feature and the line-of-sight (LOS). Applying Equation 1 to the data obtained from two viewpoints marked by the indices 1 and 2 and taking into account that  $\phi_1 = \phi_2 = \phi$ ,  $H_1 = H_2 = H$ ,  $\lambda_1 + \lambda_2 = \Delta$ , where  $\Delta$  is the separation angle between the two viewpoints, we find from these two equations

$$\cot \lambda_1 = \left( \frac{h_2 + R_{\odot} \cos \phi}{h_1 + R_{\odot} \cos \phi} + \cos \Delta \right) \frac{1}{\sin \Delta}. \quad (2)$$

Since the LOS for both instruments was directed along the prominence axis, the visible prominence tops did not necessarily show the same point of the

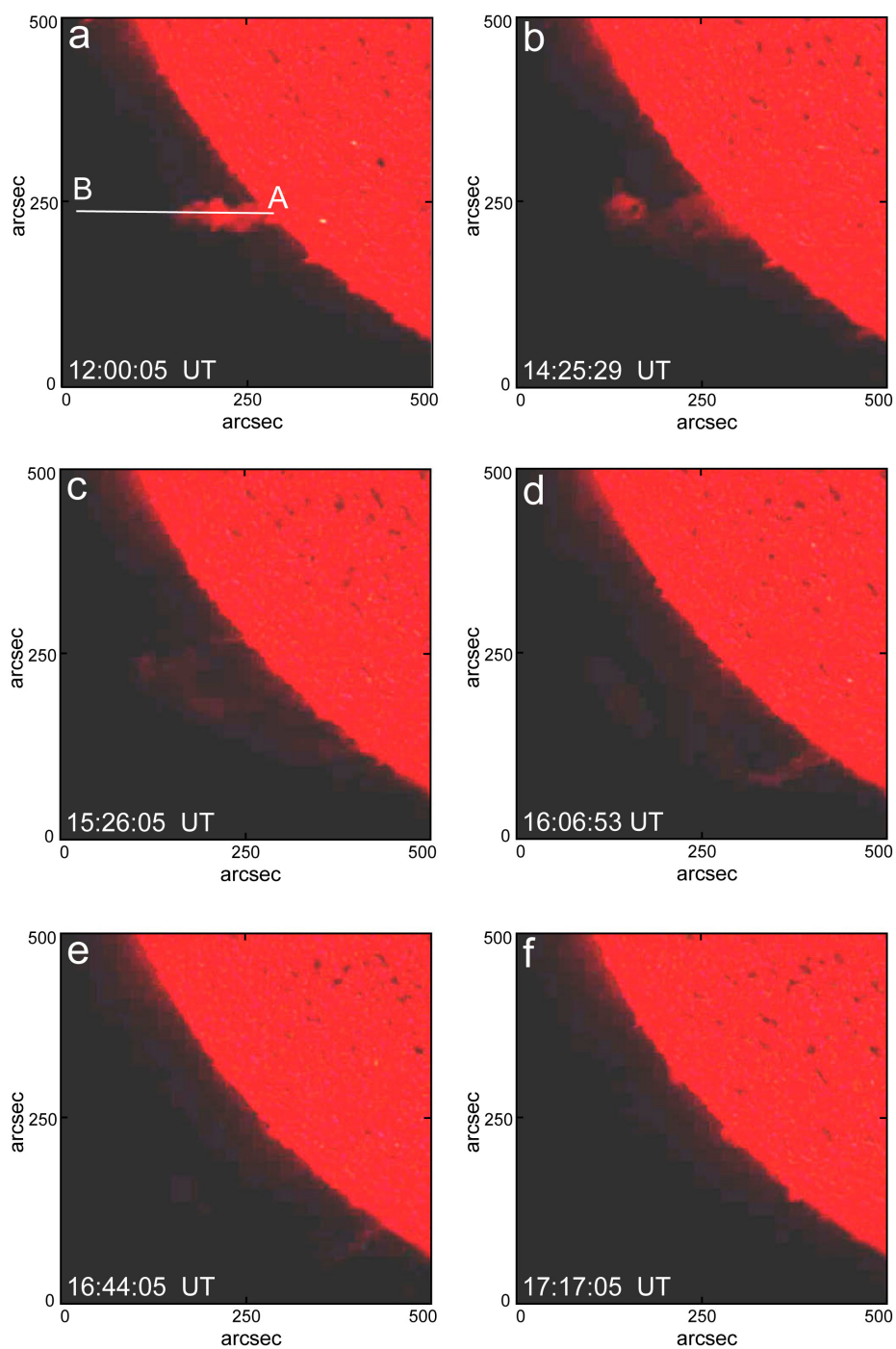


**Figure 3.** SDO/AIA 304 Å sequence showing the prominence eruption of 21 August 2017. At the time of totality of the TSE (17:24 UT), the prominence is barely seen. The *line AB* shows the slit position for the distance–time–diagram presented in Figure 4. (Courtesy of the SDO/AIA science team)



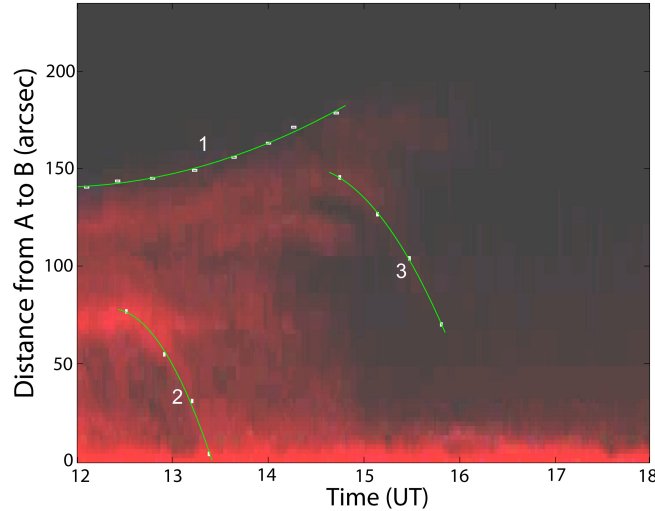


**Figure 4.** Distance–time diagram along the slit AB shown in Figure 3a. *White rectangles* show some selected points in the map. Time of the TSE is 17:24 UT. *Green lines* present second order polynomial fits to the points.

prominence spine. Figure 7 illustrates the position of the instruments relative to the prominence. Thin solid lines represent LOSs touching the prominence spine at 12:00 UT, while dashed lines correspond to the moment 15:30 UT when the prominence was erupting. If the lines touch the spine at the same point marked by the small green circle “a”, its longitude is  $\lambda_a = 72^\circ$ . However, they can touch the spine at different points as it is shown in Figure 7. The intersections of the SDO LOS with the spine are marked by crosses, while the same for STA are marked by Xs. When the prominence axis has low curvature, the intersection points are widely separated.

The prominence started to rise very slowly with a low acceleration as is seen in distance–time diagrams in Figures 4 and 6 obtained along the slits shown in Figures 3a and 5c. Green lines show second-order polynomial fits to points marking the top of the prominence

$$d = a + bt + ct^2 . \quad (3)$$

Parameters  $a$ ,  $b$ , and  $c$  are presented in Table 1 with the standard deviations for  $d$  in km above the limb and  $t$  in seconds. Acceleration is a little bit higher in the STA FOV but does not exceed  $0.8 \pm 0.1 \text{ m s}^{-2}$ . The prominence is visible longer for STA, and the final speed at 17:30 UT is  $v_{\text{STA}} = 20 \pm 2 \text{ km s}^{-1}$  at the projected height of about  $h_{\text{STA}} = 250 \text{ Mm}$ . In the SDO FOV, the filament fades out after 15:30 UT at the projected height  $h_{\text{SDO}} = 140 \text{ Mm}$ . The final speed is  $v_{\text{SDO}} = 7 \pm 2 \text{ km s}^{-1}$ . At that time  $v_{\text{STA}} = 15 \pm 2 \text{ km s}^{-1}$  and  $h_{\text{STA}} = 140 \text{ Mm}$ . It should be noted that these velocities are obtained on the basis of the distance-

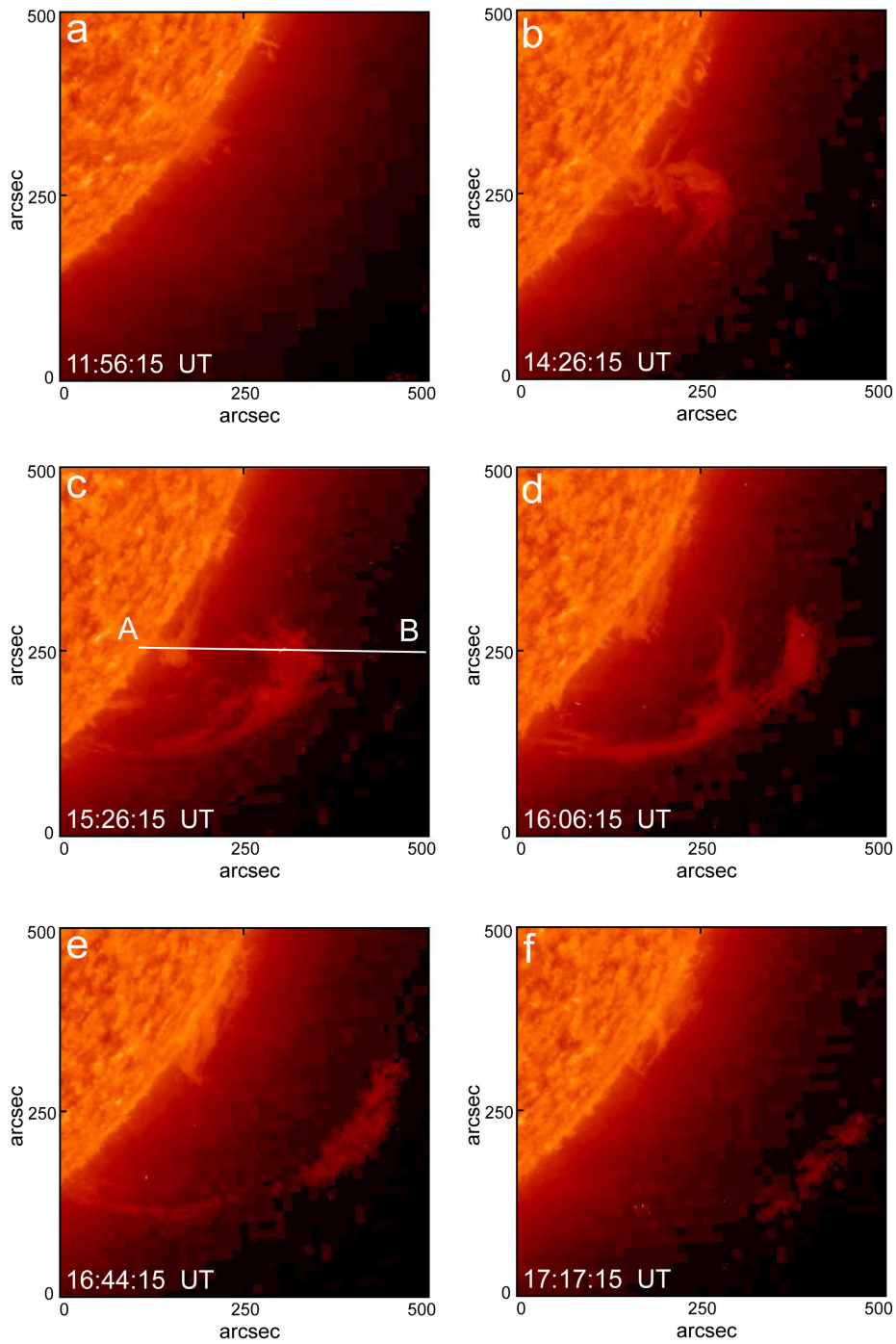


**Figure 5.** STEREO-A/EUVI 304 Å images showing the prominence eruption on 21 August 2017. The *line AB* shows the slit position for the distance–time–diagram presented in Figure 6. (Courtesy of the STEREO-A/EUVI science team)

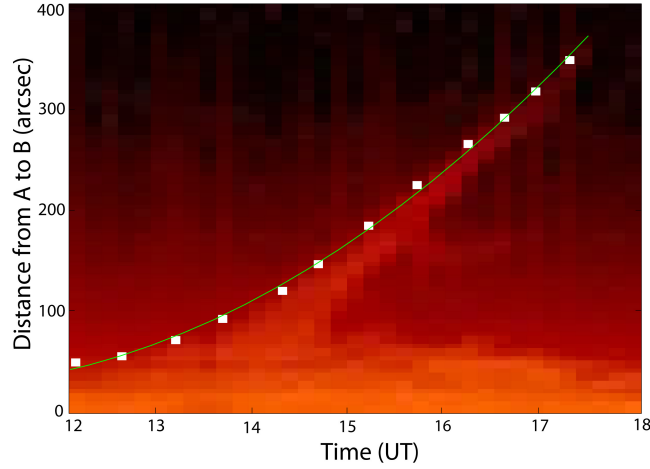


**Figure 6.** Distance–time diagram along the slit AB shown in Figure 5c.

time diagrams with the slits parallel to the Equator. Speeds and accelerations in the radial direction can be calculated by the multiplication by  $\cos \phi$ .

The highest intersections of the LOSs at 15:30 UT is marked in Figure 7 by the small green circle “b”. The corresponding longitude is  $\lambda_b = 64^\circ$ . The displacement  $l$  from the point “a” to the point “b” can be found from the triangle aOb (Figure 7) using the cosine rule

$$l = \sqrt{r_a^2 + r_b^2 - 2r_a r_b \cos(\lambda_a - \lambda_b)}, \quad (4)$$

where  $r_a = H_a + R_\odot$ ,  $r_b = H_b + R_\odot$ , and  $H_a$  and  $H_b$  are the true (radial) heights of the points “a” and “b”. Then, from the same triangle and the sine rule we derive the direction of displacement defined by the angle  $\lambda_h$

$$\lambda_h = \lambda_b - 180^\circ + \arcsin \frac{r_b \sin(\lambda_a - \lambda_b)}{l}. \quad (5)$$

Using the values presented above we obtain  $\lambda_h = 28^\circ$ .

On the other hand, we have the velocities of the prominence top derived from the displacement–time plots. If they correspond to projections of the true speed on the sky-planes of each instrument, we can find from geometry presented in Figure 7 the direction of the true motion from expression analogous to Equation 2:

$$\cot \lambda_v = \left( \frac{v_{\text{STA}}}{v_{\text{SDO}}} + \cos \Delta \right) \frac{1}{\sin \Delta}, \quad (6)$$

which gives us  $\lambda_v = 27^\circ$ . Thus, the two estimated directions of motion are nearly the same, which shows that the prominence spine points recorded as the tops by the instruments from the different viewpoints are close to each other.

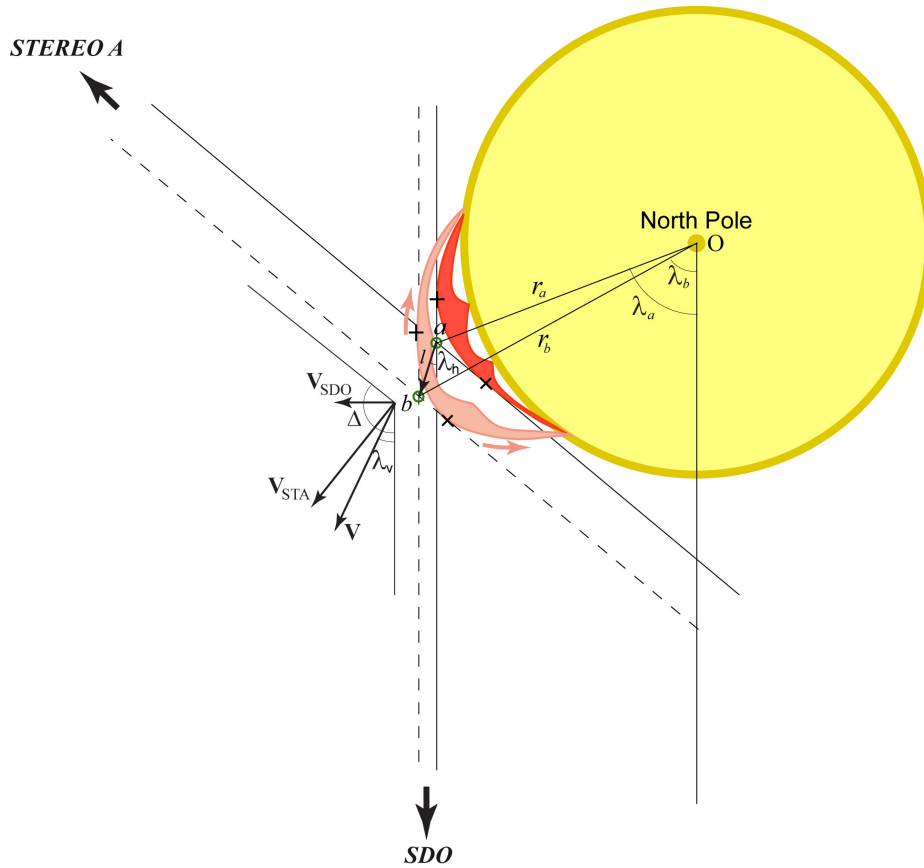


**Figure 7.** Schematic of the possible position of the prominence relative to the viewpoints of SDO and STEREO spacecraft. The *yellow circle* represents the section of the Sun at the latitude of  $-40^\circ$ . *Red and pink arches* show the prominence in the initial state and during the eruption, respectively.

No prominence plasma moving upward is visible either in SDO/AIA or STEREO/EUVI observations after 17:30 UT. The prominence disappears in the STA FOV at the height of about  $6'$  (Figures 5f and 6). Remnants of the eruptive prominence are recognized in coronal W-L images as small reddish features having this colour evidently due to  $H\alpha$  and  $D_3$  emissions. They are indicated by black arrows in Figure 2a. The prominence remnants do not show any measurable displacement during the totality, as seen in Movie 1 and Figure 2b. However, the projected radial height of the lower reddish remnant of the filament is 115 Mm, which is nearly the same as the height of the last recognizable fragment of the prominence in the SDO FOV; the height of another remnant is 200 Mm. It belongs to the upper parts of the prominence, and hence the displacement from 16 UT corresponds to a radial speed of  $20 \text{ km s}^{-1}$ .

During the slow ascending motion of the prominence, its material is observed to drain down to the surface. Most of the material is drained down along the southern leg of the visible arch. Accordingly, the supposed geometry (Figure

**Table 1.** Parameters of the second-order polynomial fits to the height–time curves of Figures 4, 6, and 9

Curve	$a$ ( $10^3$ )	$b$	$c$ ( $10^{-3}$ )
SDO/AIA 304 Å - 1	$99 \pm 1$	$7.7 \pm 0.6$	$0.26 \pm 0.05$
SDO/AIA 304 Å - 2	$51 \pm 2.5$	$-5.9 \pm 5.4$	$-7.4 \pm 2.5$
SDO/AIA 304 Å - 3	$104 \pm 1$	$-9.0 \pm 1.5$	$-3.9 \pm 0.5$
STA/EUVI 304 Å	$17 \pm 3$	$4.7 \pm 0.7$	$0.41 \pm 0.04$
SDO/AIA 171 Å	$120 \pm 1$	$3.1 \pm 0.3$	$0.19 \pm 0.024$

7) shows that the material falls down to the western end of the prominence arch, which is at the same time more southward. In SDO/AIA images, the material drops on the disc along the western leg causing some brightenings on the surface, while in STEREO/EUVI images it disappears behind the limb. In Figure 4, several descending trajectories can be recognised. The two most prominent trajectories marked as curve 2 and curve 3 show a projected acceleration of  $15 \pm 5 \text{ m s}^{-2}$  and  $8 \pm 1 \text{ m s}^{-2}$ , respectively. The projected speed at the lower parts of each curves is about  $35 \text{ km s}^{-1}$ . The downward acceleration is more than an order of magnitude higher than the upward acceleration of the erupting prominence spine. On the other hand, the downward acceleration is more than an order of magnitude lower than the free-fall acceleration ( $\approx 270 \text{ m s}^{-2}$ ), which shows that blobs fall down along gently sloping magnetic field lines.

Flow speeds in the leg are similar in SDO and STA FOVs. The most prominent blob near the limb in the STA FOV is observed within the time interval 16:24–16:44 UT with the average speed of about  $100 \text{ km s}^{-1}$ . The most prominent blob near the limb in the SDO FOV is observed within the time interval 16:09 - 16:19 UT with the average speed of about  $70 \text{ km s}^{-1}$ . It is possibly the same blob but at a greater height according to the suggested geometry (Figure 7) and it is moving at this time along a more gently sloping trajectory.

#### 4. Coronal-loop Motion and the Slow CME

In the EUV coronal channels showing a hotter plasma than what is visible in the transition-region line of the 304 Å channel, the ascending motion of coronal structures started also at about 12:00 UT (Figures 8 and 9, Movie 4). Since the polar crown prominences are associated with magnetic-flux ropes stretched in the East-West direction by the differential rotation, the flux rope axis is close to the LOS at the limb. This is a favourable position to observe coronal cavity surrounding a prominence; it could represent the internal part of the flux rope (Gibson *et al.*, 2006; Habbal *et al.*, 2010; Kucera *et al.*, 2012; Reeves *et al.*, 2012; Karna, Pesnell, and Zhang, 2015). The prominence top is located somewhere in the middle of the cavity. The U-shaped feature marked by the white arrow in Figure 8 presumably represents the lower edge of the cavity. The structure is very similar to the ones reported by Régnier, Walsh, and Alexander (2011) and

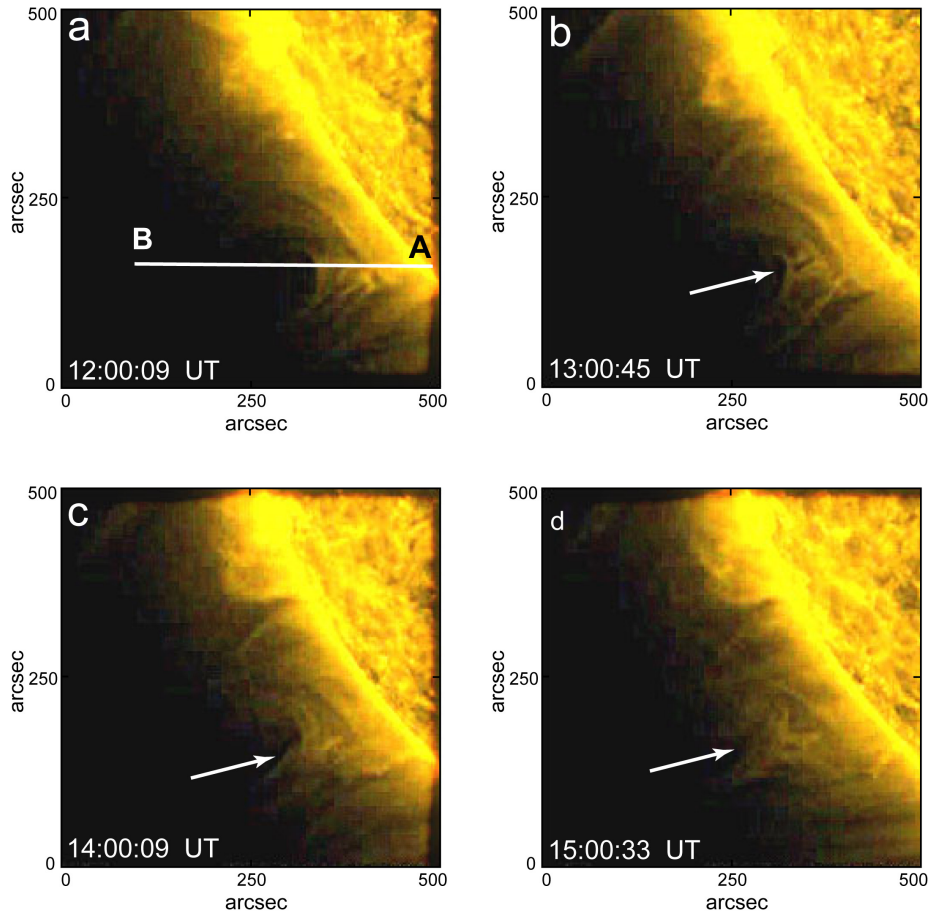


**Figure 8.** SDO/AIA 171 Å images showing the rising of the dark cavity and the coronal loops on 21 August 2017. The *line AB* shows the slit position for the distance–time-diagram presented in Figure 9. (Courtesy of the SDO/AIA science team)

Su *et al.* (2015). Different parts of a cavity usually move with different speeds during an eruption, since the cavity ascends as a whole and expands (Long *et al.*, 2018). Thus, the lower part moves with the lowest speed, while the upper part rises with the highest speed. The projected speed of the U-shaped feature is a little lower than  $10 \text{ km s}^{-1}$  (Figure 9, Table 1), which is similar to that of the prominence top (Figure 4). The upper part of the cavity is not visible in EUV images. While the cold prominence arch seems to disappear mostly due to the draining of the material toward the chromosphere, the hotter coronal structures fade away close to the upper boundary of the SDO/AIA FOV. There are no data about the evolution of the structure in the interval between the SDO/AIA FOV and the edge of the occulting disc of the SOHO/LASCO-C2 except for the moment of totality at Unity around 17:24 UT.

According to the SOHO/LASCO CME Catalog [cdaw.gsfc.nasa.gov/CME\\_list/](http://cdaw.gsfc.nasa.gov/CME_list/), a CME associated with this event appeared in the FOV of the C2 coronagraph

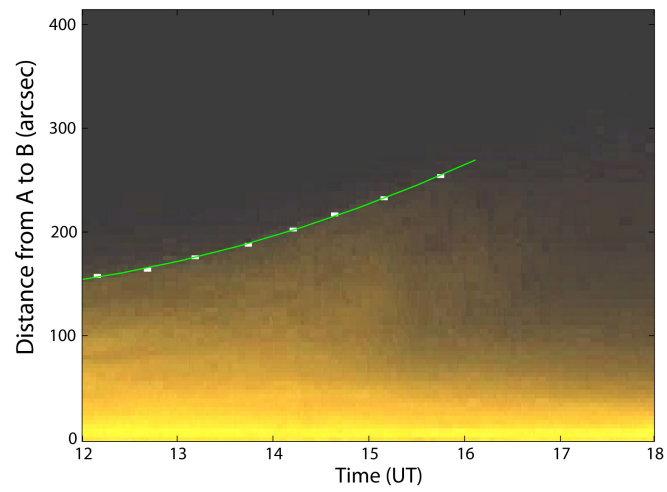


**Figure 9.** Distance–time diagram along the slit AB shown in Figure 8a.

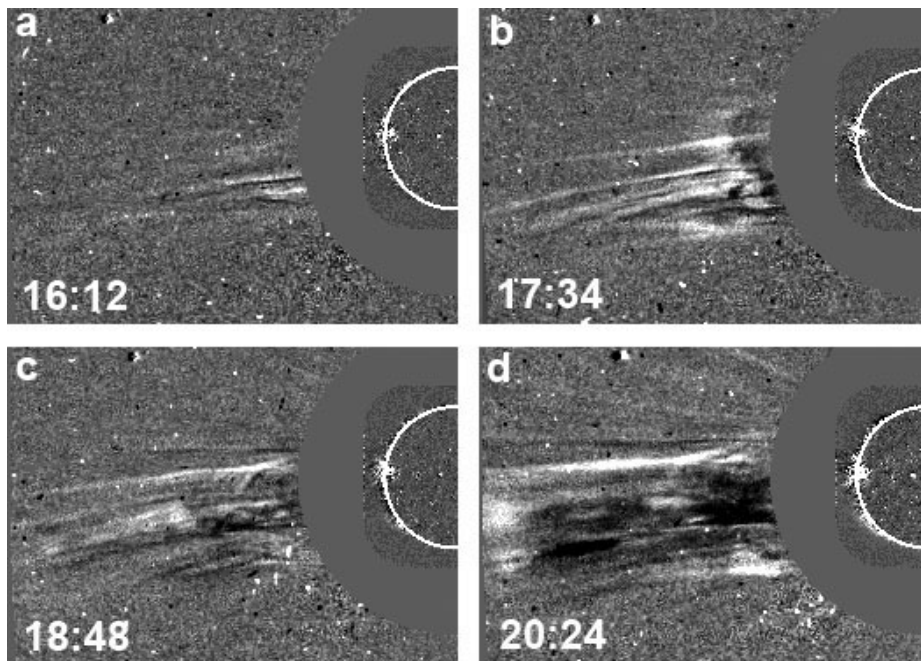


**Figure 10.** SOHO/LASCO-C2 difference images on 21 August 2017 with SDO/AIA 193 Å difference images placed at the location of the disk of the Sun. (Courtesy of the SOHO/LASCO and SDO/AIA science teams)

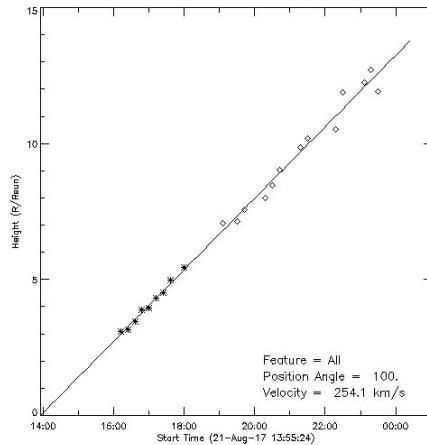


**Figure 11.** Linear fit to SOHO/LASCO observations of the E-limb CME on 21 August 2017 from the SOHO/LASCO CME Catalog ([cdaw.gsfc.nasa.gov/CME\\_list/](http://cdaw.gsfc.nasa.gov/CME_list/)). Velocities taken from the Brussels CACTus catalog (see [sidc.oma.be/cactus/](http://sidc.oma.be/cactus/)) give a large dispersion around the same typical value given here.

at 16:12 UT (Figure 10). The CME moved in the SOHO/LASCO FOV from 3 to 15  $R_{\odot}$  with a nearly constant speed of  $250 \text{ km s}^{-1}$  (Figure 11). It had neither a prominent frontal loop nor a bright core. The start time of the CME is estimated in the Catalog as 14 UT, which is close to the conspicuous prominence activation. We assume this CME to be the continuation of the slow prominence eruption. Although there are no continuous observations of the event from the low corona to the coronagraph FOV, the W-L observations fill the gap between the SDO/AIA and SOHO/LASCO observations. The W-L eclipse images (Figure 2, Movie 1) show several coronal features moving with a speed of about  $250 \text{ km s}^{-1}$  at distances of  $0.8\text{--}1.3 R_{\odot}$ . It suggests that the flux rope has accelerated after leaving the SDO/AIA FOV. However, in the SDO/AIA images the lower parts of the flux rope with the U-shape are visible, while in the W-L images the curvature of the features is directed downward, which implies that they belong to the upper parts of the flux rope or that they are pushed away by the surrounding magnetic loops and evolve synchronously as suggested by the Electronic Supplementary Material movie. As was mentioned, the lower part of an erupting flux rope always moves with a lower speed, while the upper part rises with a higher speed.

## 5. Evaluation of the Density Excess and of the Mass of the CME

Using the absolute photometry of the well-exposed W-L image, it is possible to compute the electron densities corresponding to the intensities in excess of the CME identified in Figure 2 and well observed when crossing the FOV of the LASCO-C2 coronagraph (see Figure 10). The method used to deduce electron



densities and the needed formula are given in textbooks (*e.g.* Shklovskii, 1965; Zirin, 1966; Billings, 1966) and an extended discussion of the inversion question to deduce densities, including the needed formula were given by November and Koutchmy (1996). The important parameters that are needed to extract from the coronal image are the absolute values of intensity excess measured over the background corona along the features of the CME defined as a definitely moving set of elongated features (blobs or clouds or fragments of loops) (see Figure 2). Recently such evaluation was performed for the plasma cloud corresponding to a failed small scale ejection observed at the TSE of 2010 (Tavabi, Koutchmy, and Bazin, 2018) at a radial distance near  $1.7 R_{\odot}$ . A more general and simple presentation is given by Koutchmy (1994).

We selected an original image from the set of images taken near the middle of the totality and performed an absolute calibration of this image using well-known bright stars of the FOV following the method developed for photographic pictures taken at TSE using a neutral radial filter by Koutchmy *et al.* (1978) and Lebecq, Koutchmy, and Stellmacher (1985). Some selected original images are available from the site [bass2000.obspm.fr/piwigo/index.php?/category/141](http://bass2000.obspm.fr/piwigo/index.php?/category/141). We now have digital 16-bit images composed from frames taken with different exposure times using a linear detector, which makes the work easier. The details of this photometric analysis are beyond the scope of this work and they will be given in an article in preparation. Absolute intensities of the K+F+S corona were deduced. K corresponds to the electron corona due to the Thomson scattering, F is the so-called dust corona due to the Mie scattering on particles orbiting the Sun and intercepted along the LOS, and S is the light due to the eclipse sky at totality and the eventual stray light easily evaluated using the intensity background measured on the disk of the Moon (Koutchmy *et al.*, 1978). The excess intensities corresponding to the structure that we identified with the CME are found in the range of 3 to 6% of the background intensities, and it is then easy to deduce the corresponding excess electron density [ $n_e^{\text{CME}}$ ] making the usual assumptions for computing the summed intensity along the LOS.

We assumed that the effective thickness of the CME structure is typically 14 Mm ( $1/50 R_{\odot}$ ) and extends over 420 Mm ( $0.6 R_{\odot}$ ) at an average radial distance of  $1.85 R_{\odot}$  where the effective length of integration along the LOS is  $2 R_{\odot}$  (November and Koutchmy, 1996). Using our calibrated radial scans made at the latitude where the CME structure is identified, we deduced a background  $n_e$  density of  $0.2 \times 10^7 \text{ cm}^{-3}$  at  $r = 1.75 R_{\odot}$ . The average density in the CME structure is then of order of  $(0.8 \pm 0.2) \times 10^7 \text{ cm}^{-3}$ . This is a weighted average value taking into account both the radial variations and the azimuthal variations making the turbulent structure of the CME as caught on our TSE images. With these assumptions we deduced an overall mass of the eclipse CME at the SE (excess over the background local corona) of  $1.6 \times 10^{12} \text{ g}$ . It seems to be the first evaluation of the mass of a CME made in the range of radial distances under  $2 R_{\odot}$ . We note that the CME catalogue assembled at NRL does not provide the mass of CMEs observed in 2017–18 as determined from the LASCO images; in any case they are the mass of CMEs at radial distances significantly greater than  $2.5 R_{\odot}$  as observed after subtracting a minimum background resulting from a full coronal rotation. At a radial distance of  $1.75 R_{\odot}$  the CME structure is

made of pieces that are not all definitely showing an outward motion such that our estimate of mass corresponds to an upper limit (Vourlidas *et al.*, 2010). It makes this CME a low mass CME (in the NRL terminology they would call it a poor CME) in addition to being a low-velocity one. Its morphology seems to suggest that it is the continuation of a process of outward flow of streamer sheets that occurs above the polar-crown filament and forms the shape of the classical streamer (see, *e.g.*, Koutchmy and Molodensky, 2005). The mass is clearly much lower than the mass of the erupted prominence.

## 6. Discussion

The study of CMEs is difficult due to the origin of the event from a source region in the lower corona not observed in W-L in the FOV of the externally occulted space-based coronagraphs. SDO/AIA observes up to  $0.3-0.5 R_{\odot}$  above the limb (depending on a position angle, because the detector is square) in EUV-lines reflecting different temperature regions. Images of the corona obtained using the Sun Watcher using Active Pixel System detector and Image Processing (SWAP) telescope onboard the *Project for Onboard Autonomy* (PROBA2: Berghmans *et al.*, 2006) has a slightly larger FOV but there is still a spatial gap between EUV observations and the inner boundary of SOHO/LASCO-C2 observations. In principle, the gap is covered by ground-based observations with the COronal Solar Magnetism Observatory (COSMO) K-coronagraph (K-Cor) at the Mauna Loa Solar Observatory (MLSO) in Hawaii having a FOV from  $1.05$  to  $3 R_{\odot}$  but they have a rather limited spatial resolution ( $\approx 6''$ ) and, of course, daytime and weather limitations (Hou, de Wijn, and Tomczyk, 2013).

TSEs provide the unique opportunity to observe the corona from low heights with good resolution. The observations are limited by the short period of totality at a specific ground-site and by the number of these sites along the path of the Moon shadow. Sometimes CMEs with conspicuous structure are seen in eclipse coronal images as, *e.g.*, during the 03 November 2013 eclipse. An eclipse CME was studied at the time of solar maximum (Koutchmy *et al.*, 2004). However, it is usually difficult to recognize faint CMEs in W-L eclipse coronal images at solar minimum. Our new temporal sequence of high-resolution images taken during the totality in 2017 at a single site allows one to find rapid changes in the coronal structure and to identify a CME. Observations of this unique TSE and our image processing ([hdr-astrophotography.com/](http://hdr-astrophotography.com/)) offered this opportunity for the first time.

Polar crown prominences, being stretched along heliographic parallels, can be viewed “end on” at the limb. Coronal cavities surrounding polar-crown prominences are often observed in these locations because the LOS is directed along the cavity long axis. On 21 August 2017, a cavity manifested itself by a void in EUV emission and by U-shaped threads at the bottom of the cavity. It is widely understood that a cavity is the result of the helical magnetic-field lines of a flux rope. The lower parts of these field lines are observed as U-shaped structures in  $171 \text{ \AA}$  images. The lowest sections of the helices with dips may be filled with colder dense plasma of a prominence.

Some instability of the flux rope causes it to erupt. We are not able to reach any conclusion about the type of instability (kink, torus, loss of equilibrium) based on the coronal magnetic field calculations because photospheric fields are weak below the polar-crown prominences and the surface of the photosphere make an acute angle with the LOS due to the closeness to the Pole and to the limb. Different photospheric changes can destabilize the flux rope. Usually, new magnetic-flux emergence (Sterling, Harra, and Moore, 2007; Choudhary *et al.*, 2013), magnetic-flux cancellation (Litvinenko and Martin, 1999; Yardley *et al.*, 2016), photospheric plasma flows (Roudier *et al.*, 2008, 2018), and turbulence in the prominence (Koutchmy *et al.*, 2004) are considered as triggers of the eruption. We believe that the flux rope moves under the action of forces that controlled its equilibrium before the eruption, namely the Lorentz force, consisting of the holding part from the coronal magnetic field and the supporting part from the diamagnetic photosphere, and gravity (van Tend and Kuperus, 1978; Molodenskii and Filippov, 1987; Priest and Forbes, 1990). Among them, only the diamagnetic force, which is often considered as interaction with the mirror image of the flux rope in the photosphere, is directed outward and accelerates plasma. The gravity can play a role in this process, since we deal with a rather slow process, and small cool blobs are observed returning to the surface .

Prominence material is also rising, but when the previously mostly straight axis of the flux rope becomes arch-like, the dips become too shallow and the material can drain down to the chromosphere. The prominence seems to fail to erupt since it fades out during the ascent before it reaches the FOV of the STEREO/EUVI. However, in contrast to many failed prominence eruptions, which are not followed by CMEs (Filippov and Koutchmy, 2002; Ji *et al.*, 2003; Liu *et al.*, 2009; Guo *et al.*, 2010; Joshi *et al.*, 2014), the eruption on 21 August 2017 produced a faint, slow CME. Kuridze *et al.* (2013) reported a slow CME observed after a prominence eruption, which failed or was too weak to be studied in detail. Tavabi, Koutchmy, and Bazin (2018) analyzed a slow CME event that also happened during a total solar eclipse. It was the 11 July 2010 eclipse. A small plasma blob or plasmoid was observed in EUV slowly accelerating up to a speed of  $12 \text{ km s}^{-1}$ , then slowing down and stopped at a height of about 500 Mm in the corona. The blob was captured in W-L eclipse observations and the evaluated density of the blob is significantly bigger than what we evaluated in this event.

Since the hot coronal structures were too faint to follow them near the upper boundary of the SDO/AIA FOV, it is not easy to decide whether the whole flux rope stopped in the middle corona as in two-step eruptions (Filippov and Koutchmy, 2002; Byrne *et al.*, 2014; Gosain *et al.*, 2016; Wang *et al.*, 2016; Chandra *et al.*, 2017). However, the observed mass-unloading within the prominence arch favours the flux rope scenario with acceleration as is suggested in mass-unloading eruption scenarios (Klimchuk, 2001; Zhou *et al.*, 2006; Jenkins *et al.*, 2018). If gravitation is significant in the flux-rope equilibrium, the acceleration after its violation cannot exceed the acceleration due to gravity [ $g = 270 \text{ m s}^{-2}$ ]. In such a process, only a rather slow CME can be produced, as is the case in the 21 August 2017 event. The high-quality W-L coronal images obtained during the total eclipse prove that the erupting flux rope was present and moved in

the corona after leaving the EUV telescope FOV and before the appearance in the coronagraph FOV. They allowed us to recognize a number of small coronal features moving outward in the south-east sector of the corona during the short period of the totality and the presence of the prominence remnants at higher level than what was observed in the EUV.

## 7. Summary and Conclusions

We analyzed the temporal changes within the SE part of the TSE solar corona before, during, and after the total solar eclipse on 21 August 2017. Short displacements of a number of coronal features were definitely found for the first time in W-L coronal images taken during the totality from observations made at a single observation site. Special image processing allows us to reveal these changes. They represent synchronous motion of the features away from the Sun with a speed of about  $250 \text{ km s}^{-1}$ . The comparison with observations from space-based instruments onboard SDO, STEREO-A, and SOHO showed that the features belong to a slow CME propagating through the corona. SDO/AIA and STEREO-A/EUVI observations in the  $304 \text{ \AA}$  channels showed a slow prominence eruption starting well before the totality. The prominence rose with a speed of the order of  $10 \text{ km s}^{-1}$ . The prominence material was observed to drain down to the chromosphere along the prominence arch preferentially to the south-west endpoint of the prominence.

SDO/AIA  $171 \text{ \AA}$  images show a coronal cavity around the initial position of the prominence. The lower edge of the cavity represented by the U-shaped structure ascended together with the prominence with a similar speed. We identify the cavity with the magnetic-flux rope containing the cool dense prominence material in dips at the bottom of presumably helical field lines. The flux rope lost its equilibrium and started to erupt due to some instability that we cannot specify on the basis of the available observations.

SOHO/LASCO data showed a slow CME propagating in the range from 3 to  $15 R_{\odot}$  with a nearly constant speed of  $250 \text{ km s}^{-1}$ . It shows neither a prominent frontal loop nor a bright core. The start time of the CME is close to the beginning of the prominence activation. We assume this CME to be the continuation of the very slow prominence eruption. The draining down of the prominence material, possibly, unloaded the flux rope and allowed it to accelerate more energetically upward to form the slow CME. The slow CME speed and its low acceleration support this scenario because the driving force is comparable with the gravity force and the possible acceleration cannot exceed the gravity acceleration. The movie assembled during the short interval of totality of the eclipse observed at a single site with the same instrument (Movie 1) confirms this picture, suggesting that a whole set of the magnetic structures above the E-limb are indeed involved. Apparently, observations taken by different instruments along the path of totality did not provide a really useful comparison in order to improve the result of this analysis from a single-site observations taken with the excellent resolution. We found that it is important to use the same method and the same instrumental parameters to deduce relevant parameters. The forthcoming ESA space mission

PROBA 3 with its ASPIICS coronagraph (Lamy *et al.*, 2008; Renotte *et al.*, 2015; Shestov, Zhukov, and Seaton, 2019) is well suited to tackle the questions that we left unresolved.

**Acknowledgements** The authors thank the SOHO, the STEREO, and the SDO scientific teams for the high-quality data they supply. The CME catalog is generated and maintained at the CDAW Data Center by NASA and The Catholic University of America in cooperation with the Naval Research Laboratory. SOHO is a project of international cooperation between ESA and NASA. STEREO is the third mission in NASA's Solar Terrestrial Probes program. SDO is a mission of NASA's Living With a Star Program. Some movies were created using the ESA and NASA funded Helioviewer Project.

## Disclosure of Potential Conflicts of Interest

The authors declare that they have no conflicts of interest.

## References

- Airapetian, V.S., Koutchmy, S.: 1994, Fast coronal transient (CME) with twisted legs. In: Hunt, J.J. (ed.) *Solar Dynamic Phenomena and Solar Wind Consequences, the Third SOHO Workshop*, **SP-373**, ESA, Noordwijk, 195. ADS.
- Banterle, F., Artusi, A., Debattista, K., Chalmers, A.: 2018, *Advanced High Dynamic Range Imaging*, A K Peters/CRC Press, Natick, Massachusetts.
- Berghmans, D., Hochedez, J.F., Defise, J.M., Lecat, J.H., Nicula, B., Slemzin, V., Lawrence, G., Katsyiannis, A.C., van der Linden, R., Zhukov, A., Clette, F., Rochus, P., Mazy, E., Thibert, T., Nicolosi, P., Pelizzo, M.-G., Schühle, U.: 2006, SWAP onboard PROBA 2, a new EUV imager for solar monitoring. *Adv. Space Res.* **38**, 1807. DOI. ADS.
- Billings, D.E.: 1966, *A guide to the solar corona*, Academic Press, New York. ADS.
- Boulade, S., Delannée, C., Koutchmy, S., Lamy, P., Llebaria, A., Howard, R., Schwenn, R., Simnett, G.: 1997, Analysis of a High Latitude Slow CME with Travelling Ejecta. In: Wilson, A. (ed.) *Fifth SOHO Workshop: The Corona and Solar Wind Near Minimum Activity* **SP-404**, ESA, Noordwijk, 217. ADS.
- Brueckner, G.E., Howard, R.A., Koomen, M.J., Korendyke, C.M., Michels, D.J., Moses, J.D., Socker, D.G., Dere, K.P., Lamy, P.L., Llebaria, A., Bout, M.V., Schwenn, R., Simnett, G.M., Bedford, D.K., Eyles, C.J.: 1995, The Large Angle Spectroscopic Coronagraph (LASCO). *Solar Phys.* **162**, 357. DOI. ADS.
- Bugoslavskaja, E.I.: 1949, Struktura solnechnoi korony. *Trudy Gosudarstvennogo Astronomicheskogo Instituta* **19**. ADS.
- Byrne, J.P., Morgan, H., Seaton, D.B., Bain, H.M., Habbal, S.R.: 2014, Bridging EUV and White-Light Observations to Inspect the Initiation Phase of a “Two-Stage” Solar Eruptive Event. *Solar Phys.* **289**, 4545. DOI. ADS.
- Chandra, R., Filippov, B., Joshi, R., Schmieder, B.: 2017, Two-Step Filament Eruption During 14 - 15 March 2015. *Solar Phys.* **292**, 81. DOI. ADS.
- Chen, J., Krall, J.: 2003, Acceleration of coronal mass ejections. *J. Geophys. Res. (Space Phys.)* **108**, 1410. DOI. ADS.
- Cheng, X., Ding, M.D., Guo, Y., Zhang, J., Vourlidas, A., Liu, Y.D., Olmedo, O., Sun, J.Q., Li, C.: 2014, Tracking the Evolution of a Coherent Magnetic Flux Rope Continuously from the Inner to the Outer Corona. *Astrophys. J.* **780**, 28. DOI. ADS.
- Choudhary, D.P., Gosain, S., Gopalswamy, N., Manoharan, P.K., Chandra, R., Uddin, W., Srivastava, A.K., Yashiro, S., Joshi, N.C., Kayshap, P., Dwivedi, V.C., Mahalakshmi, K., Elamathi, E., Norris, M., Awasthi, A.K., Jain, R.: 2013, Flux emergence, flux imbalance, magnetic free energy and solar flares. *Adv. Space Res.* **52**, 1561. DOI. ADS.
- Cliver, E.W.: 1989, Was the eclipse comet of 1893 a disconnected coronal mass ejection? *Solar Phys.* **122**, 319. DOI. ADS.

- Delaboudinière, J.-P., Artzner, G.E., Brunaud, J., Gabriel, A.H., Hochedez, J.F., Millier, F., Song, X.Y., Au, B., Dere, K.P., Howard, R.A., Kreplin, R., Michels, D.J., Moses, J.D., Defise, J.M., Jamar, C., Rochus, P., Chauvineau, J.P., Marioge, J.P., Catura, R.C., Lemen, J.R., Shing, L., Stern, R.A., Gurman, J.B., Neupert, W.M., Maucherat, A., Clette, F., Cugnon, P., van Dessel, E.L.: 1995, EIT: Extreme-Ultraviolet Imaging Telescope for the SOHO Mission. *Solar Phys.* **162**, 291. DOI. ADS.
- Druckmüller, M., Rušin, V., Minarovjech, M.: 2006, A new numerical method of total solar eclipse photography processing. *Contributions of the Astronomical Observatory Skalnaté Pleso* **36**(3), 131. ADS.
- Eddy, J.A.: 1974, A Nineteenth-century Coronal Transient. *Astron. Astrophys.* **34**, 235. ADS.
- Feynman, J., Ruzmaikin, A.: 2004, A High-Speed Erupting-Prominence CME: A Bridge Between Types. *Solar Phys.* **219**, 301. DOI. ADS.
- Filippov, B., Koutchmy, S.: 2002, About the prominence heating mechanisms during its eruptive phase. *Solar Phys.* **208**, 283. DOI. ADS.
- Filippov, B.P.: 2013, Height of a solar filament before eruption. *Astron. Rep.* **57**, 778. DOI. ADS.
- Foley, C.R., Harra, L.K., Matthews, S.A., Culhane, J.L., Kitai, R.: 2003, Evidence for a Flux Rope driven EUV wave and CME: Comparison with the Piston Shock Model. *Astron. Astrophys.* **399**, 749. DOI. ADS.
- Gibson, S.E., Foster, D., Burkepile, J., de Toma, G., Stanger, A.: 2006, The Calm before the Storm: The Link between Quiescent Cavities and Coronal Mass Ejections. *Astrophys. J.* **641**, 590. DOI. ADS.
- Gopalswamy, N.: 2004, A Global Picture of CMEs in the Inner Heliosphere. In: Poletto, G., Suess, S.T. (eds.) *The Sun and the Heliosphere as an Integrated System*, *Astrophys. Space Sci. Lib.* **317**, 201. DOI. ADS.
- Gosain, S., Filippov, B., Ajoy Maurya, R., Chandra, R.: 2016, Interrupted Eruption of Large Quiescent Filament Associated with a Halo CME. *Astrophys. J.* **821**, 85. DOI. ADS.
- Guo, Y., Ding, M.D., Schmieder, B., Li, H., Török, T., Wiegmann, T.: 2010, Driving Mechanism and Onset Condition of a Confined Eruption. *Astrophys. J. Lett.* **725**, L38. DOI. ADS.
- Habbal, S.R., Druckmüller, M., Morgan, H., Scholl, I., Rušin, V., Daw, A., Johnson, J., Arndt, M.: 2010, Total Solar Eclipse Observations of Hot Prominence Shrouds. *Astrophys. J.* **719**, 1362. DOI. ADS.
- Hanaoka, Y., Nakazawa, J., Ohgoe, O., Sakai, Y., Shiota, K.: 2014, Coronal Mass Ejections Observed at the Total Solar Eclipse on 13 November 2012. *Solar Phys.* **289**, 2587. DOI. ADS.
- Hou, J., de Wijn, A.G., Tomczyk, S.: 2013, Design and measurement of the Stokes polarimeter for the COSMO K-coronagraph. *Astrophys. J.* **774**, 85. DOI. ADS.
- House, L.L., Wagner, W.J., Hildner, E., Sawyer, C., Schmidt, H.U.: 1981, Studies of the corona with the Solar Maximum Mission coronagraph/polarimeter. *Astrophys. J. Lett.* **244**, L117. DOI. ADS.
- Howard, R.A., Moses, J.D., Vourlidas, A., Newmark, J.S., Socker, D.G., Plunkett, S.P., Korndyke, C.M., Cook, J.W., Hurley, A., Davila, J.M., Thompson, W.T., St Cyr, O.C., Mentzell, E., Mehalick, K., Lemen, J.R., Wuelsel, J.P., Duncan, D.W., Tarbell, T.D., Wolfson, C.J., Moore, A., Harrison, R.A., Waltham, N.R., Lang, J., Davis, C.J., Eyles, C.J., Mapson-Menard, H., Simnett, G.M., Halain, J.P., Defise, J.M., Mazy, E., Rochus, P., Mercier, R., Ravet, M.F., Delmotte, F., Auchere, F., Delaboudinière, J.P., Bothmer, V., Deutsch, W., Wang, D., Rich, N., Cooper, S., Stephens, V., Maahs, G., Baugh, R., McMullin, D., Carter, T.: 2008, Sun Earth Connection Coronal and Heliospheric Investigation (SECCHI). *Space Sci. Rev.* **136**, 67. DOI. ADS.
- Illing, R.M.E., Hundhausen, A.J.: 1985, Observation of a coronal transient from 1.2 to 6 solar radii. *J. Geophys. Res.* **90**, 275. DOI. ADS.
- Jenkins, J.M., Long, D.M., van Driel-Gesztelyi, L., Carlyle, J.: 2018, Understanding the Role of Mass-Unloading in a Filament Eruption. *Solar Phys.* **293**, 7. DOI. ADS.
- Ji, H., Wang, H., Schmahl, E.J., Moon, Y.-J., Jiang, Y.: 2003, Observations of the Failed Eruption of a Filament. *Astrophys. J. Lett.* **595**, L135. DOI. ADS.
- Joshi, N.C., Srivastava, A.K., Filippov, B., Kayshap, P., Uddin, W., Chandra, R., Prasad Choudhary, D., Dwivedi, B.N.: 2014, Confined Partial Filament Eruption and its Reformation within a Stable Magnetic Flux Rope. *Astrophys. J.* **787**, 11. DOI. ADS.
- Karna, N., Pesnell, W.D., Zhang, J.: 2015, Appearances and Statistics of Coronal Cavities During the Ascending Phase of Solar Cycle 24. *Astrophys. J.* **810**, 123. DOI. ADS.

- Klimchuk, J.A.: 2001, Theory of Coronal Mass Ejections. *Washington DC American Geophysical Union Geophysical Monograph Series* **125**. DOI. ADS.
- Koutchmy, S.: 1994, Coronal physics from eclipse observations. *Advances in Space Research* **14**(4), 29. DOI. ADS.
- Koutchmy, S., Fagot, J.: 1973, Rapid Variations Observed during the Total Eclipse of the Sun on June 30, 1973. *Nature* **246**, 414. DOI. ADS.
- Koutchmy, S.L., Molodensky, M.M.: 2005, Magnetic Configurations of Streamer Structures in the Solar Atmosphere. *Astron. Lett.* **31**, 398. DOI. ADS.
- Koutchmy, S., Stellmacher, G., Koutchmy, O., Dzubenko, N.I., Ivanchuk, V.I., Popov, O.S., Rubo, G.A., Vsekhsviatskii, S.K., Lamy, P.: 1978, Photometrical analysis of the June 30, 1973 solar corona. *Astron. Astrophys.* **69**, 35. ADS.
- Koutchmy, S., Baudin, F., Bocchialini, K., Daniel, J.-Y., Delaboudinière, J.-P., Golub, L., Lamy, P., Adjabshirizadeh, A.: 2004, The August 11th, 1999 CME. *Astron. Astrophys.* **420**, 709. DOI. ADS.
- Kucera, T.A., Gibson, S.E., Schmit, D.J., Landi, E., Tripathi, D.: 2012, Temperature and Extreme-ultraviolet Intensity in a Coronal Prominence Cavity and Streamer. *Astrophys. J.* **757**, 73. DOI. ADS.
- Kuridze, D., Mathioudakis, M., Kowalski, A.F., Keys, P.H., Jess, D.B., Balasubramaniam, K.S., Keenan, F.P.: 2013, Failed filament eruption inside a coronal mass ejection in active region 11121. *Astron. Astrophys.* **552**, A55. DOI. ADS.
- Lamy, P., Vivès, S., Damé, L., Koutchmy, S.: 2008, *New perspectives in solar coronagraphy offered by formation flying: from PROBA-3 to Cosmic Vision*, CS-7010, Soc. Photo-Optical Instrum. Eng. (SPIE), Bellingham, WA, 70101H. DOI. ADS.
- Lebecq, C., Koutchmy, S., Stellmacher, G.: 1985, The 1981 total solar eclipse corona. II. Global absolute photometric analysis. *Astron. Astrophys.* **152**, 157. ADS.
- Lemen, J.R., Title, A.M., Akin, D.J., Boerner, P.F., Chou, C., Drake, J.F., Duncan, D.W., Edwards, C.G., Friedlaender, F.M., Heyman, G.F., Hurlburt, N.E., Katz, N.L., Kushner, G.D., Levay, M., Lindgren, R.W., Mathur, D.P., McFeaters, E.L., Mitchell, S., Rehse, R.A., Schrijver, C.J., Springer, L.A., Stern, R.A., Tarbell, T.D., Wuelser, J.-P., Wolfson, C.J., Yanari, C., Bookbinder, J.A., Cheimets, P.N., Caldwell, D., Deluca, E.E., Gates, R., Golub, L., Park, S., Podgorski, W.A., Bush, R.I., Scherrer, P.H., Gumm, M.A., Smith, P., Auken, G., Jerram, P., Pool, P., Souffi, R., Windt, D.L., Beardsley, S., Clapp, M., Lang, J., Waltham, N.: 2012, The Atmospheric Imaging Assembly (AIA) on the Solar Dynamics Observatory (SDO). *Solar Phys.* **275**, 17. DOI. ADS.
- Li, T., Zhang, J.: 2015, High-Resolution Observations of a Flux Rope with the Interface Region Imaging Spectrograph. *Solar Phys.* **290**, 2857. DOI. ADS.
- Litvinenko, Y.E., Martin, S.F.: 1999, Magnetic reconnection as the cause of a photospheric canceling feature and mass flows in a filament. *Solar Phys.* **190**, 45. DOI. ADS.
- Liu, Y., Su, J., Xu, Z., Lin, H., Shibata, K., Kurokawa, H.: 2009, New Observation of Failed Filament Eruptions: The Influence of Asymmetric Coronal Background Fields on Solar Eruptions. *Astrophys. J. Lett.* **696**, L70. DOI. ADS.
- Long, D.M., Harra, L.K., Matthews, S.A., Warren, H.P., Lee, K.-S., Doschek, G.A., Hara, H., Jenkins, J.M.: 2018, Plasma Evolution within an Erupting Coronal Cavity. *Astrophys. J.* **855**, 74. DOI. ADS.
- Molodenskii, M.M., Filippov, B.P.: 1987, Rapid Motion of Filaments in Solar Active Regions - Part Two. *Soviet Astron.* **31**, 564. ADS.
- November, L.J., Koutchmy, S.: 1996, White-Light Coronal Dark Threads and Density Fine Structure. *Astrophys. J.* **466**, 512. DOI. ADS.
- Priest, E.R., Forbes, T.G.: 1990, Magnetic field evolution during prominence eruptions and two-ribbon flares. *Solar Phys.* **126**, 319. DOI. ADS.
- Reeves, K.K., Gibson, S.E., Kucera, T.A., Hudson, H.S., Kano, R.: 2012, Thermal Properties of a Solar Coronal Cavity Observed with the X-Ray Telescope on Hinode. *Astrophys. J.* **746**, 146. DOI. ADS.
- Régnier, S., Walsh, R.W., Alexander, C.E.: 2011, A new look at a polar crown cavity as observed by SDO/AIA. Structure and dynamics. *Astron. Astrophys.* **533**, L1. DOI. ADS.
- Renotte, E., Alia, A., Bemporad, A., Bernier, J., Bramanti, C., Buckley, S., Capobianco, G., Cernica, I., Dániel, V., Darakchiev, R., Darmetko, M., Debaize, A., Denis, F., Desselle, R., de Vos, L., Dinescu, A., Fineschi, S., Fleury-Frenette, K., Focardi, M., Fumel, A., Galano, D., Galy, C., Gillis, J.-M., Górski, T., Graas, E., Graczyk, R., Grochowski, K., Halain, J.-P.A., Hermans, A., Howard, R., Jackson, C., Janssen, E., Kasprzyk, H., Kosiec, J., Koutchmy, S., Kovačičinová, J., Kranitis, N., Kurowski, M., Ladno, M., Lamy, P., Landini,

- F., Lapáček, R., Lédl, V., Liebecq, S., Loreggia, D., McGarvey, B., Massone, G., Melich, R., Mestreau-Garreau, A., Mollet, D., Mosdorf, L., Mosdorf, M., Mroczkowski, M., Muller, R., Nicolini, G., Nicula, B., O'Neill, K., Orleński, P., Palau, M.-C., Pancrazzi, M., Paschalis, A., Patočka, K., Peresty, R., Popescu, I., Psota, P., Rataj, M., Rautakoski, J., Romoli, M., Rybecký, R., Salvador, L., Servaye, J.-S., Solomon, C., Stockman, Y., Swat, A., Thizy, C., Thomé, M., Tsinganos, K., Van der Meulen, J., Van Vooren, N., Vit, T., Walczak, T., Zarzycka, A., Zender, J., Zhukov, A.: 2015, *Design status of ASPIICS, an externally occulted coronagraph for PROBA-3*, **CS-9604**, Soc. Photo-Optical Instrum. Eng. (SPIE), Bellingham, WA, 96040A. DOI. ADS.
- Roudier, T., Švanda, M., Meunier, N., Keil, S., Rieutord, M., Malherbe, J.M., Rondi, S., Molodij, G., Bommier, V., Schmieder, B.: 2008, Large-scale horizontal flows in the solar photosphere. III. Effects on filament destabilization. *Astron. Astrophys.* **480**, 255. DOI. ADS.
- Roudier, T., Schmieder, B., Filippov, B., Chandra, R., Malherbe, J.M.: 2018, Horizontal photospheric flows trigger a filament eruption. *Astron. Astrophys.* **618**, A43. DOI. ADS.
- Schmieder, B., Aulanier, G., Vršnak, B.: 2015, Flare-CME Models: An Observational Perspective (Invited Review). *Solar Phys.* **290**, 3457. DOI. ADS.
- Schwenn, R.: 1996, An Essay on Terminology, Myths and Known Facts: Solar Transient - Flare - CME - Driver Gas - Piston - BDE - Magnetic Cloud - Shock Wave - Geomagnetic Storm. *Astrophys. Space Sci.* **243**, 187. DOI. ADS.
- Sheeley, J. N. R., Wang, Y.-M.: 2007, In/Out Pairs and the Detachment of Coronal Streamers. *Astrophys. J.* **655**(2), 1142. DOI. ADS.
- Sheeley, N.R., Walters, J.H., Wang, Y.-M., Howard, R.A.: 1999, Continuous tracking of coronal outflows: Two kinds of coronal mass ejections. *J. Geophys. Res.* **104**, 24739. DOI. ADS.
- Shestov, S.V., Zhukov, A.N., Seaton, D.B.: 2019, Modeling and removal of optical ghosts in the PROBA-3/ASPIICS externally occulted solar coronagraph. *Astron. Astrophys.* **622**, A101. DOI. ADS.
- Shklovskii, I.S.: 1965, *Physics of the solar corona*, Pergamon Press, Oxford. ADS.
- Srivastava, N., Schwenn, R., Inhester, B., Stenborg, G., Podlipnik, B.: 1999, Acceleration Profile of the Slow Solar Wind as Inferred from Gradual Mass Ejections Observed by LASCO. *Space Sci. Rev.* **87**, 303. DOI. ADS.
- Srivastava, N., Schwenn, R., Inhester, B., Martin, S.F., Hanaoka, Y.: 2000, Factors Related to the Origin of a Gradual Coronal Mass Ejection Associated with an Eruptive Prominence on 1998 June 21-22. *Astrophys. J.* **534**, 468. DOI. ADS.
- Sterling, A.C., Harra, L.K., Moore, R.L.: 2007, New Evidence for the Role of Emerging Flux in a Solar Filament's Slow Rise Preceding Its CME-producing Fast Eruption. *Astrophys. J.* **669**, 1359. DOI. ADS.
- Su, Y., van Ballegooijen, A., McCauley, P., Ji, H., Reeves, K.K., DeLuca, E.E.: 2015, Magnetic Structure and Dynamics of the Erupting Solar Polar Crown Prominence on 2012 March 12. *Astrophys. J.* **807**, 144. DOI. ADS.
- Tavabi, E., Koutchmy, S., Bazin, C.: 2018, Analysis of a Failed Eclipse Plasma Ejection Using EUV Observations. *Solar Phys.* **293**, 42. DOI. ADS.
- Tousey, R.: 1973, The solar corona. In: Rycroft, M.J., Runcorn, S.K. (eds.) *Space Res. Conf.* **2**, 713. ADS.
- van Tend, W., Kuperus, M.: 1978, The development of coronal electric current systems in active regions and their relation to filaments and flares. *Solar Phys.* **59**, 115. DOI. ADS.
- Vourlidas, A., Howard, R.A., Esfandiari, E., Patsourakos, S., Yashiro, S., Michalek, G.: 2010, Comprehensive Analysis of Coronal Mass Ejection Mass and Energy Properties Over a Full Solar Cycle. *Astrophys. J.* **722**(2), 1522. DOI. ADS.
- Vršnak, B., Sudar, D., Ruždjak, D.: 2005, The CME-flare relationship: Are there really two types of CMEs? *Astron. Astrophys.* **435**, 1149. DOI. ADS.
- Vršnak, B., Maričić, D., Stanger, A.L., Veronig, A.: 2004, Coronal Mass Ejection of 15 May 2001: II. Coupling of the Cme Acceleration and the Flare Energy Release. *Solar Phys.* **225**, 355. DOI. ADS.
- Wagner, W.J.: 1984, Coronal Mass Ejections. *Ann. Rev. Astron. Astrophys.* **22**, 267. DOI. ADS.
- Wang, R., Liu, Y.D., Zimovets, I., Hu, H., Dai, X., Yang, Z.: 2016, Sympathetic Solar Filament Eruptions. *Astrophys. J. Lett.* **827**, L12. DOI. ADS.
- Wueller, J.-P., Lemen, J.R., Tarbell, T.D., Wolfson, C.J., Cannon, J.C., Carpenter, B.A., Duncan, D.W., Gradwohl, G.S., Meyer, S.B., Moore, A.S., Navarro, R.L., Pearson, J.D.,



- Rossi, G.R., Springer, L.A., Howard, R.A., Moses, J.D., Newmark, J.S., Delaboudiniere, J.-P., Artzner, G.E., Auchere, F., Bougnet, M., Bouyries, P., Bridou, F., Clotaire, J.-Y., Colas, G., Delmotte, F., Jerome, A., Lamare, M., Mercier, R., Mullet, M., Ravet, M.-F., Song, X., Bothmer, V., Deutsch, W.: 2004, EUVI: the STEREO-SECCHI extreme ultraviolet imager. In: Fineschi, S., Gummin, M.A. (eds.) *Telescopes and Instrumentation for Solar Astrophysics, Proc. SPIE* **5171**, 111. DOI. ADS.
- Yardley, S.L., Green, L.M., Williams, D.R., van Driel-Gesztelyi, L., Valori, G., Dacie, S.: 2016, Flux Cancellation and the Evolution of the Eruptive Filament of 2011 June 7. *Astrophys. J.* **827**, 151. DOI. ADS.
- Zhang, J., Dere, K.P., Howard, R.A., Kundu, M.R., White, S.M.: 2001, On the Temporal Relationship between Coronal Mass Ejections and Flares. *Astrophys. J.* **559**, 452. DOI. ADS.
- Zhou, G.P., Wang, J.X., Zhang, J., Chen, P.F., Ji, H.S., Dere, K.: 2006, Two Successive Coronal Mass Ejections Driven by the Kink and Drainage Instabilities of an Eruptive Prominence. *Astrophys. J.* **651**, 1238. DOI. ADS.
- Zirin, H.: 1966, *The solar atmosphere*, Blaisdell Pub. Company,, Waltham- Massachusetts-Toronto- London. ADS.